Iron Solids Formed from Oxidation Precipitation of Ferrous Sulfate Solutions

Mfandaidza Hove, Robert P. van Hille, and Alison E. Lewis
Dept. of Chemical Engineering, University of Cape Town, Private Bag Rondebosch 7701, South Africa

DOI 10.1002/aic.11264
Published online August 17, 2007 in Wiley InterScience (www.interscience.wiley.com).

The oxidation and precipitation of iron from ferrous sulfate solutions was studied at high Fe^{2+} concentrations, as found in typical South African acid mine drainage, and at high pH, as practised in the removal of iron from acid mine drainage (AMD) by the high-density sludge process. The results obtained showed that the nature of the precipitates formed was largely determined by the rate of Fe^{2+} oxidation. High pH promoted higher-oxidation rates resulting in high-nucleation rates, and the consequent formation of finer particles. The precipitation process in all cases was found to produce nano-sized, growth limited primary particles. These primary particles later aggregated, producing particles several hundreds of nanometres in size. At pH 8.0, these fine particles aggregated due to Van der Waals forces, while at pH 10.0, ferrihydrite was found to transform into goethite. The settling rates of the precipitates showed little dependence on the pH. The precipitate formed at pH 6.0 contained consistently higher proportions of Fe^{2+} compared to the precipitates formed at higher pHs. Interestingly, particles formed at higher pH gave lower final BET surface areas, contrary to the trend that would be predicted from the evolution of the population based average particle size.
 AIChE J, 53: 2569–2577, 2007
Keywords: acid mine drainage, high-density sludge process, iron oxidation precipitation

Introduction

The mining of sulfide ores often results in the disturbance of the geological strata and the generation of pyrite containing waste and tails. Contact between pyrite minerals, water and air results in abiotic and biotic oxidation, which releases sulfate (SO_4^{2-}), ferrous iron (Fe^{2+}) and protons (H^+). The acid formed causes the mobilization of other acid labile heavy metals, resulting in an acidic water stream that is heavy. The Fe^{2+} can oxidize into Fe^{3+}, which then hydrolyzes into "ferric hydroxides"

$$\text{Oxidation reaction} \quad 4Fe^{2+}(aq) + O_2(g) + 4H^+(aq) \leftrightarrow 4Fe^{3+}(aq) + 2H_2O(1) \qquad (1)$$

$$\text{Hydrolysis} \quad Fe^{3+}(aq) + 3H_2O(1) \leftrightarrow Fe(OH)_3(s) + 3H^+(aq) \qquad (2)$$

Correspondence concerning this article should be addressed to M. Hove at mfandaidza.hove@uct.ac.za.

The combined oxidation and precipitation of iron as shown in the aforementioned equations is employed in the treatment of acid mine drainage by the so called high-density sludge (HDS) process.[2,3] In this process, the ferrous iron is first oxidized according to Eq. 1, by bubbling air through the metal-laden wastewater at a pH ranging from 8.5 to 9.5.[4] The rate of the forward reaction in Eq. 1 increases by 100-fold for every unit change in the pH in systems with pH above five.[5] The same reaction has been found to increase by approximately 10-fold for every 15°C increase in temperature,[5] due to the dependence of the ionic product of water and the hydroxyl ion concentration on temperature. The ferric iron and other metals are then precipitated by adding lime to maintain the pH around 9.5. This is followed by the addition of flocculating polymers to increase solids density and finally, clarification. Solids obtained this way have been found to be voluminous, unstable and have poor dewatering characteristics.[3] The solids concentration rarely exceeds 4%. The cause of this poor settling, clarification and reduced potential for thickening and filtration lies in the structure of

the ferric precipitate formed. The recycling of sludge has been found to increase solids concentration considerably.[6,7] The problem in the earlier versions of the process, consisting of a simple sludge recycle stream, was that the added alkali was equally attractive to the recycled sludge as a precipitation nucleation point. The solution to this was the introduction of a preconditioning tank, where the lime and the recycled sludge were mixed together before oxidation. The recycled sludge, thus, becomes alkalized prior to entering the oxidation and neutralization tanks, thus, promoting precipitation on the surface of the recycled sludge particles. This resulted in the formation of sludge that was more dense than in the single-pass systems.

Despite the improvements cited previously, the disposal of metal-laden sludge from acid mine drainage treated by this technique still causes problems of low-solids density, long-term instability, and the need for a large land area for disposal. One of the motivations for this study was to develop a deeper understanding of the particle formation mechanisms. The study focused on two areas; first: an investigation into factors affecting the rate of oxidation of ferrous iron, which indirectly generates the supersaturation needed for solids formation, and second; an investigation into the hydrolysis and precipitation of ferric ions in alkaline aqueous systems.

The hydrolysis begins with the ejection of a proton from hexaqua ions, followed by the condensation of the resultant hydroxylated orange monomeric iron complexes to form polycationic species that are red in color.[8] The condensation occurs by either dehydration between the hydroxyl groups (olation), and the formation of hydroxo bridges between neighboring particles, or, in the absence of water molecules in the coordination sphere, the condensation takes place through a two-step associative mechanism that leads to the formation of oxo bridges.[9,10] The aggregation of these clusters is dependent on the rate of oxidation, which controls the level of supersaturation and prevailing pH conditions.[11] However, Van der Woude and De Bruyn[12] and Pavlides,[13] found that the iron particles precipitated at low pH had a limiting size, independent of the iron concentration and pH. Deprotonation of these positively charged polymeric species (also referred to as colloids) by addition of a base led to coagulation.[14] It is expected, therefore, that at high pH (6.0–10.0) larger particles will be formed, compared to those formed by Van der Woude and De Bruyn[12] and Pavlides[13] due to base induced coagulation of the precursor polynuclear species.

Due to the very low solubility of most of the ferric iron phases, very high-supersaturation levels are encountered in iron precipitation processes. The high-supersaturation levels promote aggregation in preference to growth. Although ferrihydrite is thermodynamically less stable, it has been found to be kinetically favored, relative to the more stable phases, at low pH.[15] The mechanism of ferrihydrite precipitation from homogeneous solutions at these low pHs has been found to start with the formation of nuclei, which are growth limited to about 3–5nm.[16] These nanosized particles may then aggregate to form particles larger in size.[17] All the studies cited here were performed at low pH, in the range of pH 3–5. The objective of this study was to investigate the particle process mechanisms in the formation of iron precipitates at conditions of higher pH (6.0–10.0) and high-iron concentrations, as encountered in the treatment of acid mine drainage by the high-density sludge process.

Techniques and Experimental Methods

Technique for studying particle processes

A technique that is often used to make inferences about particle formation processes during precipitation is based on the moment transformation of the number-density function $n(L)$, which is obtained by integrating the same with respect to the size of the particles L. Thus, the j^{th} moment becomes

$$m_j = \int_0^\infty L^j n(L) dL,$$

The symbols L, $n(L)$ and m_j represent the size of the particles, the number-density function of particles of size L and the moment, respectively. From the integration of the aforementioned term, the moments obtained are; zeroth moment (m_0), first moment (m_1), second moment (m_2,), and third moment (m_3), which are proportional to the total number of particles, total length of particles, total surface area of particles, and total volume of particles, respectively.[18,19] The total mass of the particles can be obtained by multiplying m_3 by the density of the particles.

When these moments are computed, they give a single important point for each of the samples taken during the course of the reaction. A plot of the various moments against time can be used to deduce the active precipitation mechanisms. This technique has been successfully used by Ntuli and Lewis,[20] Andreassen and Hounslow,[21] and Randolph and Larson.[18]

Experimental method

All the experiments were carried out in a 4 liter batch reactor, as shown in Figure 1. The reactor had four equally spaced baffles and a central draft tube in order to maximize mixing. The agitator was fitted with a Rushton turbine, and a speed of 350 rpm was used for all the experimental runs. The top of the reactor was covered by a lid with ports for electrodes to measure pH, dissolved oxygen concentration, and another port for sample collection.

The reactor was first filled with 4 L of deionized water, which was then deoxygenated using nitrogen. The pH was

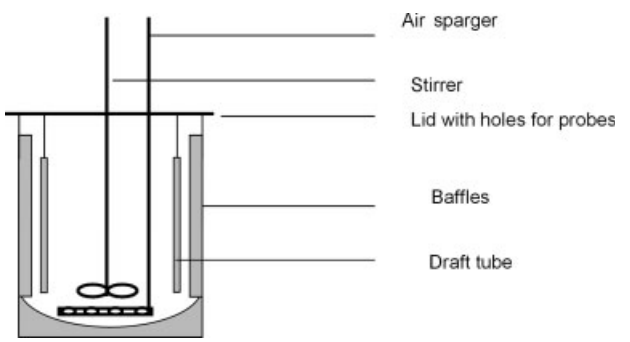

Figure 1. Experimental setup.

adjusted to the desired level by means of a custom made pH control system using a Hitech Micro Systems controller and Hanna MA911 pH electrode by injecting either 0.1 M H_2SO_4 or 0.1 M NaOH. The pH controller was calibrated against a commercial Hanna 211 meter coupled to a Hanna MA911 electrode using commercial pH buffer solutions. The accuracy of the pH stat was 0.1 pH units. Dissolved oxygen concentration was monitored by a YSI 5739 electrode coupled to a Hitech Micro Systems controller. Iron, at a concentration of 200 mg/L, was then added as $FeSO_4.7H_2O$. The air supply was opened up to a flow rate in excess of the stoichiometric oxygen requirements. After oxidation was complete and with the stirrer still running, 1 L of the sludge was transferred to an Imhoff cone and allowed to settle for 24 h, after which a sample was taken according to the procedure below for iron and solids analysis.

Samples were collected using a syringe and rapidly quenched with H_2SO_4 to pH 3.0, and deoxygenated using nitrogen to stop oxidation. One part of the sample was filtered through 0.45 μm filter paper. The filtrate was analyzed for dissolved iron ($Fe^{2+}$and total Fe) using a Merck Spectroquant® NOVA 60. The procedure for iron analysis was based on the 1–10 phenanthroline method.[22] The concentration of Fe^{3+} was found by difference. The other part of the sample was washed several times with deionized water to remove excess ions and then freeze-dried for 48 h. The resulting solids were analyzed for particle-size distribution using a Zetasizer Nano ZS series, and phases were identified using XRD techniques. A portion of these solids was digested in order to determine the quantity of iron in the solids for purposes of computing a material balance on iron. The samples were collected at different time intervals until the end of the oxidation reaction and after 1,440 min (24 h). All the experimental runs were carried out at room-temperature, and repeated several times for reproducibility. There was 23% variability in the results obtained, which is compatible with 20% variability found by other workers.[23]

Results and Discussion

Oxidation of Fe^{2+}

The plot of the Fe^{2+} concentration remaining in solution as a function of time for pH 6.0 and 9.0 is shown in Figure 2. The plots indicate the rate of oxidation to increase with an increase in pH as would be expected according to the rate laws given by Stumm and Lee.[5] The average rates of oxidation were found to be 2.1 mg(Fe^{2+})/L/Min, 4.9 mg(Fe^{2+})/L/Min, 9.8 mg(Fe^{2+})/L/Min and 19.9 mg(Fe^{2+})/L/Min at pH 6.0, 8.0, 9.0 and 10.0, respectively. For the pH 6.0 case, the average rate of oxidation obtained was more than 0.044 mg(Fe^{2+})/L/Min, which would be predicted from literature based calculations.[5] The reason for the higher than expected rate was due to the catalytic effect of ferrihydrite solids in the pH range 6.0–7.0 as found by Tamura et al.[25] and Sung and Morgan.[23] The oxidation rates found in this work for pHs 8.0, 9.0 and 10.0 are significantly lower compared to the rates that would be predicted from literature based calculations.[5] This reduced rate could be due to the increased complexity of iron speciation at higher pH.[10] It is also known that SO_4^{2-} (which is a dominating ion in this case) reduces the rate of Fe^{2+} oxidation.[23,24] It is also very likely that at higher ferrous iron concentration and higher pH, the rate law given by Stumm and Lee[5] may not hold. The rapid initial drop in Fe^{2+} concentration for all cases could have been due to direct aqueous oxidation while the slower rates toward the end of the reaction could have been due to transformation reactions involving Fe^{2+}/Fe^{3+} metastable complexes and/or Fe^{2+} adsorbed on the ferrihydrite surface.[35]

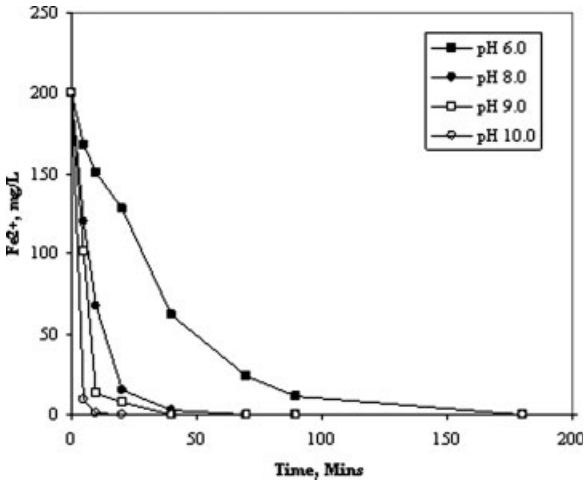

Figure 2. Fe^{2+} remaining in solution as a function of time.

Particle-Size Distribution

Solids formed after 5 min of reaction

The particle-number distribution, N, (£/m^3) of the particles formed after five minutes of reaction is shown in Figure 3. At pH 6.0 and 9.0, bimodal distributions were obtained, while unimodal distributions were obtained at pH 8.0 and 10.0. The peaks were at 1,280 nm and 4,800 nm at pH 6.0, and 459 nm and 531 nm at pH 8.0 and 10.0, respectively. The distribution at pH 9.0 showed the formation of smaller particles with peaks at 190 nm and 712 nm. The total number of particles increased with higher pH due to the increase in the amount of precipitate formed in the same time interval. The wide span of the distribution in all cases supports the initial formation of monomeric species, which condense into larger polymeric species by an aggregative mechanism.[8,26] The BET surface area (discussed in the section Evolution of BET Specific Surface Area) showed that these particles were aggregates. The open structure of the particles indicated that the solids were made up of mainly amorphous ferrihydrite, while traces of green rusts and lepidocrocite were picked up by XRD analysis. The decrease in the size of the particles at higher pH was due to the increased oxidation rate, which resulted in high-primary nucleation rates and depressed growth of the particles. These conditions of high-oxidation rate (Figure 2) support high supersaturation levels, resulting in the formation of thermodynamically less stable, but kinetically favored ferrihydrite and green rusts.[15,26] It is because of the high-oxidation rates that the number of particles formed also increased significantly at pH 9.0 compared to pH 6.0 (Figure 3b). In all cases the size of the particles

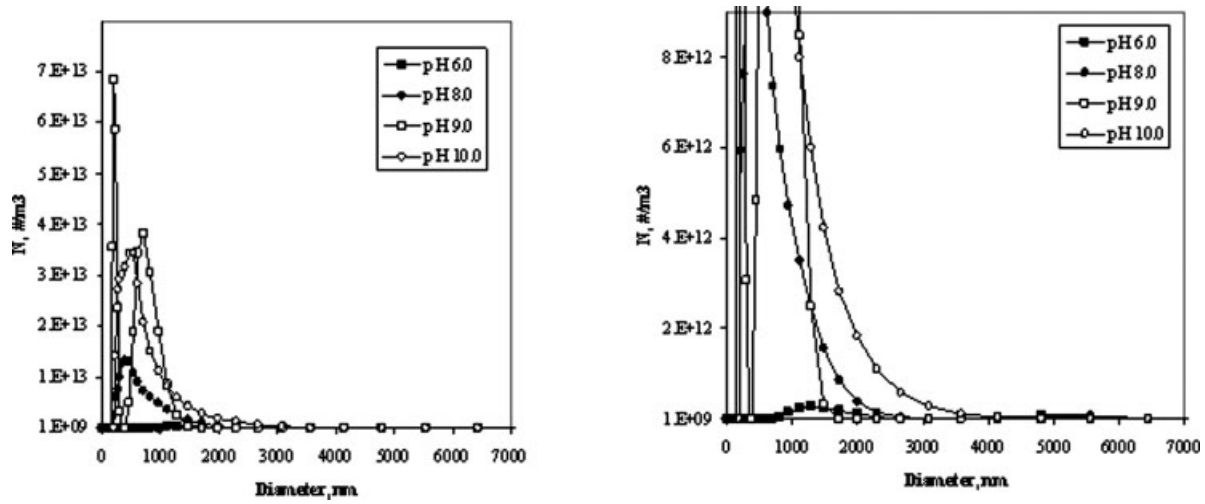

Figure 3. Particle-size distribution after 5 min of reaction.

The graph on the right is a y-axis magnification of the graph on the left in order to show the distribution at pH 6.0.

obtained was larger than the limiting colloid size, reported by Van der Woude and De Bruyn,[12] of 3–5 nm. This could have been due to the high pH (more hydroxide ions), which induced deprotonation of the polynuclear species, and led to coagulative aggregation. However, at higher pH, it would seem that the rate of deprotonation was lower than the rate of nucleation, hence, smaller particles were formed although there was more base compared to pH 6.0. The bimodal distribution obtained is typical of mixed phase systems, supporting the view that different iron phases were formed during the initial stages of the reaction.

Solids formed after 10 min of reaction

The particle-number distributions for solids formed after 10 min of reaction are shown in Figure 4. The precipitate that had formed after 10 min at pH 6.0 showed high polydispersity, with modal peaks at 396 nm, 1,720 nm and 4,800 nm. The number-density distribution of the particles formed at pH 9.0 had a modal peak of 396 nm, while that for pH 10.0 was 1,280 nm. The distribution at pH 8.0 also showed a bimodal distribution with peaks at 615 nm and 4,800 nm. The higher proportion of smaller particles at 10 min compared to 5 min was as a result of continued nucleation for the pH 6.0, 8.0 and pH 9.0 cases. The particles are much larger for pH 10.0, because the oxidation at this stage was more than 90% complete (see Figure 2). The change (at 10 min) in the particle-size distribution compared to the one at five min, could also be due to the formation of green rusts and transformation of polymeric ferrihydrite phases. Visual and XRD analysis showed that green rust complexes were formed at this stage[28] except for the pH 10.0 case.

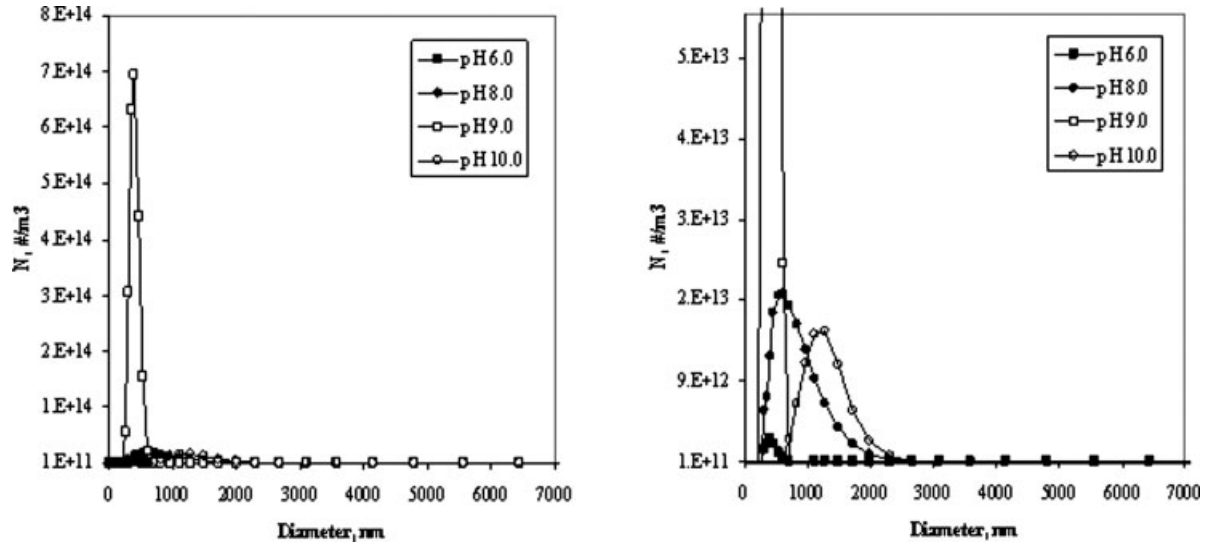

Figure 4. Particle-size distribution after 10 min of reaction.

The graph on the right is a y-axis magnification of the graph on the left in order to show distribution at pH 6.0.

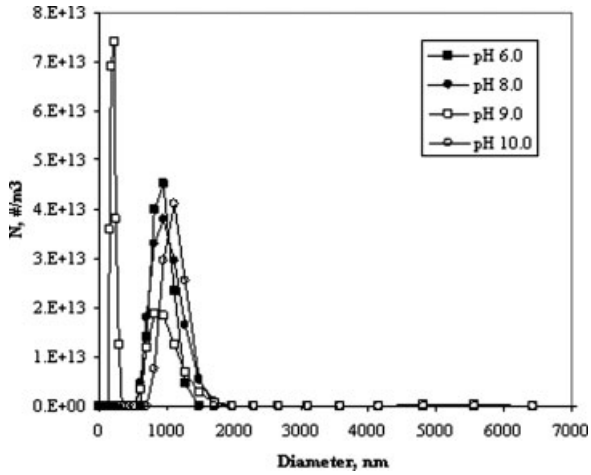

Figure 5. Particle-size distribution after 40 min of reaction.

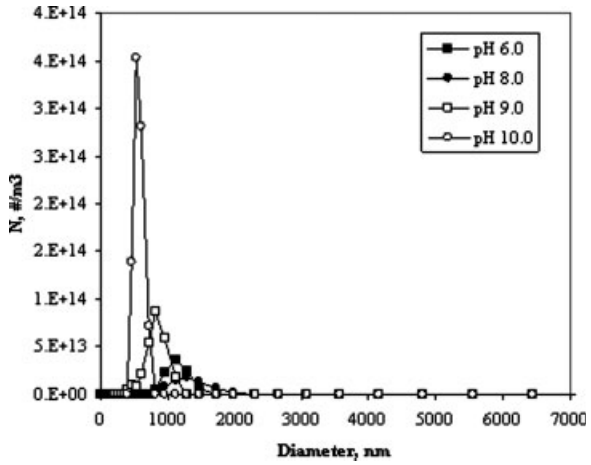

Figure 6. Particle-size distribution after 90 min of reaction.

Solids formed after 40 min of reaction

The particle-number distributions are shown in Figure 5. The particle-size distribution of the solids present at this stage of the reaction showed a narrower monomodal distributions at pH 6.0, 8.0 and 10.0 (Figure 5). The modal peaks were 955 nm, 955 nm and 1,110 nm, respectively. Two peaks (122 nm and 459 nm) were obtained at pH 9.0. The disappearance of the larger particles previously obtained at pH 6.0 and 8.0 was as a result of solution-mediated transformation of the green rusts as air continued to be bubbled through the reactor. XRD analysis confirmed the absence of green rusts in all precipitates at this stage of the reaction.[28] This disappearance of the larger particles cannot be attributed to dissolution, because the concentration of dissolved iron continued to decrease during the course of the reaction. The zeroth moment, (m_0) also increased (see Figure 10), which supports the view that there was nucleation of "new" iron species. The decrease in the size of the particles for the pH 10.0 case was clearly due to the transformation of ferrihydrite into goethite.[29] From this it can be concluded that the transformation of less stable species into more crystalline phases takes place in all cases but with the onset of the same coming earlier at pH 10.0 than at any other pH. From a wastewater treatment operation point of view this could mean that it is more beneficial (disregarding the increased mean particle size) to oxidize iron at pH 10.0, as this results in a more stable precipitate compared to oxidation at lower pH.

Solids formed after 90 min of reaction

The particle-size distribution for the precipitate present after 90 min of reaction is shown in Figure 6. The number distribution of the particles was monomodal with peak height at 1,110 nm, 1,280 and 712 nm for pH 6.0 8.0 and 9.0, respectively. The larger particle size at pH 8.0 was due to Van der Waals induced coagulation since the point of zero charge for most iron oxide hydroxides is around pH 7.0–8.0.[9] The disappearance of the smaller size particles compared to the previous distributions, and the increase in the modal size showed that the active size enlargement mechanism was aggregation for these particular pH cases. At pH 10, the modal size was 531 nm. The significantly smaller size was due to the dissolution of ferrihydrite to form the more stable goethite.[29] Thus, this stage represents the onset of "goethite nucleation".

Solids formed after 180 min of reaction

The number distribution of the particle size was monomodal with the peak at 1,110 nm, 1,480, 712 nm and 955 nm (Figure 7) for pH 6.0, 8.0, 9.0 and 10.0, respectively. The increase in the modal size at pH 10.0 was due to the growth and/or agglomeration of goethite formed from the dissolution of ferrihydrite.

Solids formed after 1,440 min (24 h) of reaction

The size distribution was narrower and monomodal with modal height at 1,720 nm, 2,300 nm, 1,280 nm and 2,670 for pH 6.0, 8.0, 9.0 and 10.0, respectively. In all cases there was a marked increase in the modal size of the particles accom-

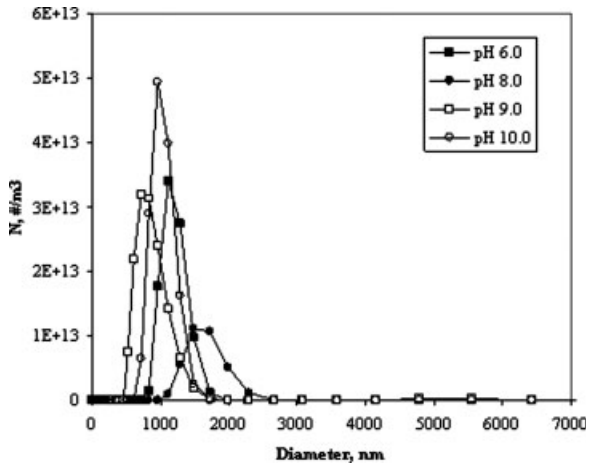

Figure 7. Particle-size distribution after 180 min of reaction.

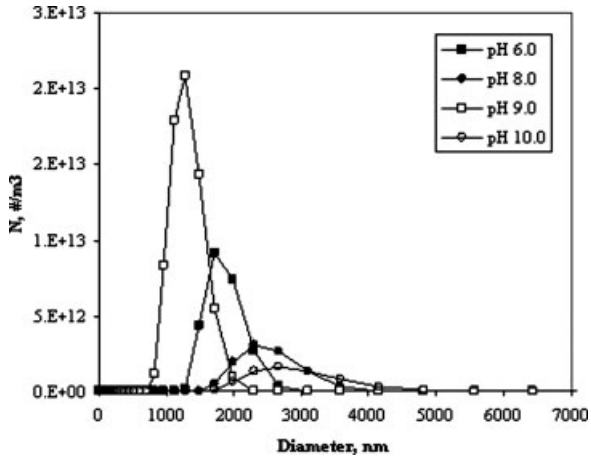

Figure 8. Particle size distribution after 1,440 min of reaction.

panied by a corresponding decrease in the number of particles. The larger particle size obtained at pH 8.0 was due to Van der Waals induced agglomeration since the point of zero charge of most iron oxide phases is around pH 7.0–8.0.[9] The distribution is shown in Figure 8.

Polydispersity and spread of the particle-size distribution

The span of the particle-size distribution for each of the samples was estimated by calculating the relative standard deviation (RSD) of each distribution according to the equation following

$$\text{RSD}\% = \frac{\text{Standard deviation}}{\text{Mean size } (\overline{\text{L}}_{1,0})} \times 100$$

The variation of the RSD for each particle-size distribution measurement is shown in Figure 9. The plot indicates that the spread and the polydispersity of the particle size decreased with time for the pH 6.0, 8.0 and 10.0 cases. This is in agreement with the observed disappearance of the bimodal distribution and the emergence of a more uniform monomodal distribution. This trend could be due to the increasing order/crystallinity of the precipitated solids with time. Considering the pH 9.0 case, although there is a general decrease in the RSD, it is not systematic as in the other cases. The lack of consistency could mean that the particle formation processes are more complex at pH 9.0 than at any other pH considered in this work.

Evolution of number of particles (m_0) and mean size of particles ($\overline{L}_{1,0}$)

The evolution of the zeroth moment (m_0) is shown in Figure 10. The increase in the total number of particles, up to 40 min for cases pH 6.0, 8.0 and 9.0, was most likely due to nucleation. While breakage would have a similar effect on m_0, this is unlikely to be the cause of the cited observation since there was always a corresponding decrease in the amount of iron in solution which indicated consumption of supersaturation. The decrease in m_0 at pH 9.0 from 40 to 90 min was sharper than at pH 6.0 and pH 8.0. This indicated that the aggregation rates were higher at pH 9.0 than at pH 6.0 and 8.0 since aggregation is the only mechanism responsible for a decrease in the number of particles in this instance. From 90 min to 1,440 min there was a continued decrease in m_0 for the three cases showing that Van der Waals forces were responsible for inducing aggregation or flocculation since there was no more supersaturation remaining in solution. For the pH 10.0 case, after five minutes of reaction, the value of m_0 had already decreased. This is expected since at this stage the oxidation of ferrous iron was almost complete.

The change of the population based mean size ($\overline{\text{L}}_{1,0}$) of the particles as a function of time is shown in Figure 11. For cases pH 6.0 and 9.0, the initial decrease in from 5 to 10 min was due to high-rates of nucleation at the expense of growth and aggregation.[28] From 10 min up to 90 min the mean particle size increased due to aggregation. This is supported by a corresponding decrease in m_0 for both cases. The near constant mean particle size between 90 and 180 min again showed that the system could have reached a state of dynamic equilibrium between particle breakage/or attrition

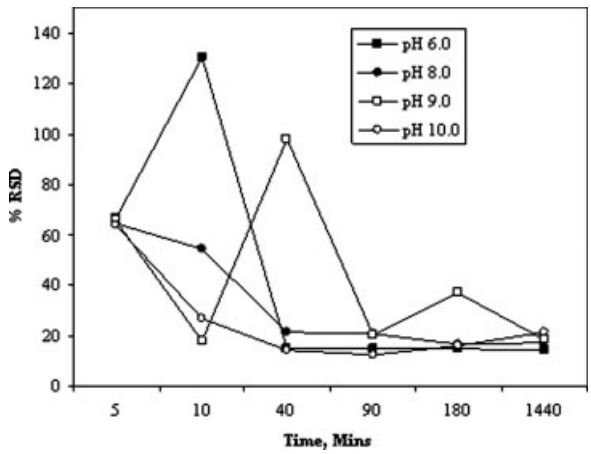

Figure 9. Variation of the RSD of the particle size distribution with time.

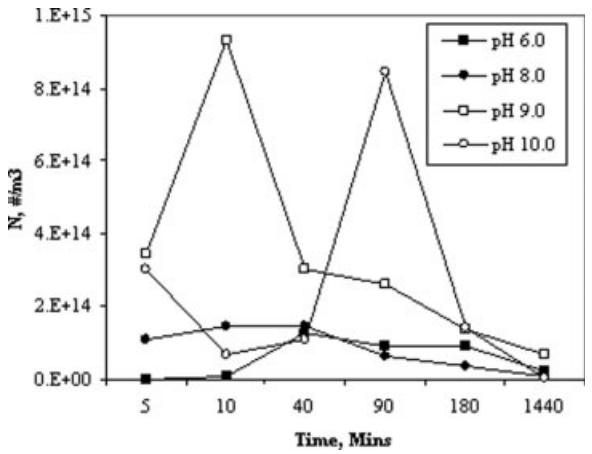

Figure 10. Evolution of m_0 during the course of the reaction.

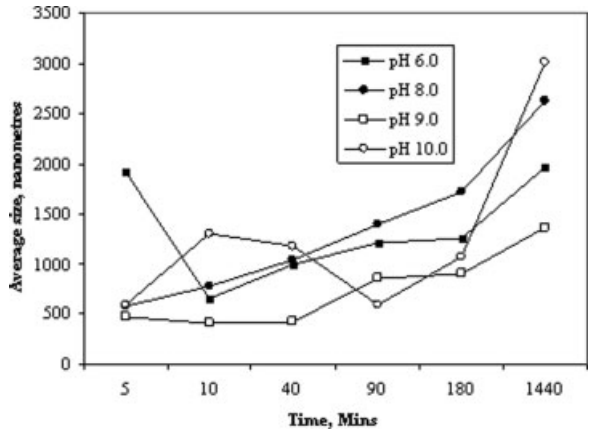

Figure 11. Evolution of population based average size during the course of the reaction.

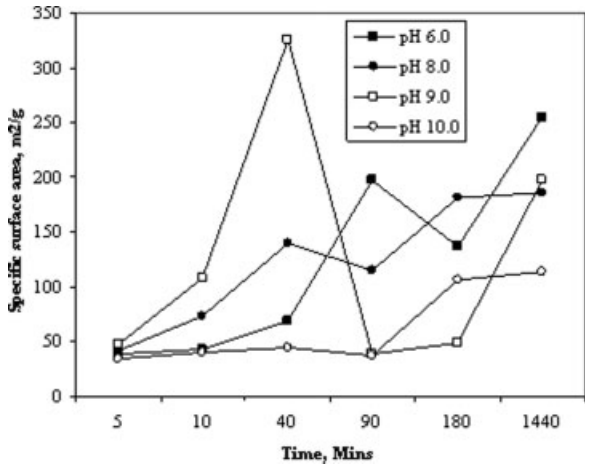

Figure 13. Evolution of the BET specific surface area during the course of the reaction.

and aggregation. For the pH 8.0 case, there was a gradual increase in the particle size up to the end of the reaction. This increase was due to Van der Waals induced aggregation (flocculation) of the iron precipitates. A decrease in the population based average size for the pH 10.0 case from 5 min to 90 min was due to the transformation of ferrihydrite into goethite. An increase in the average size from 90 min to 1,440 was due to the aggregation and/or growth of goethite. In conclusion therefore, the formation of ferrihydrite particles at pH 6.0 to 9.0 is dominated by nucleation at the initial stages followed by limited growth. Aggregation dominates after the oxidation stage has been completed. At pH 10.0, the process is dominated by aggregation of ferrihydrite at the initial stages, followed by the dissolution/reprecipitation of goethite, and finally by the aggregation of goethite.

Although the average particle sizes were different for all the cases, there was no significant improvement in the settling behavior of the bigger particles, as shown in Figure 12. The solids densities (m/v) were 0.87%, 0.92%, 0.85 and 0.90% for pH 6.0, 8.0, 9.0 and 10.0, respectively. From these values, the implication is that it is more favorable to operate these processes at the higher pH and, thereby, benefit from the kinetic advantages, given that the settling behavior hardly changes with pH.

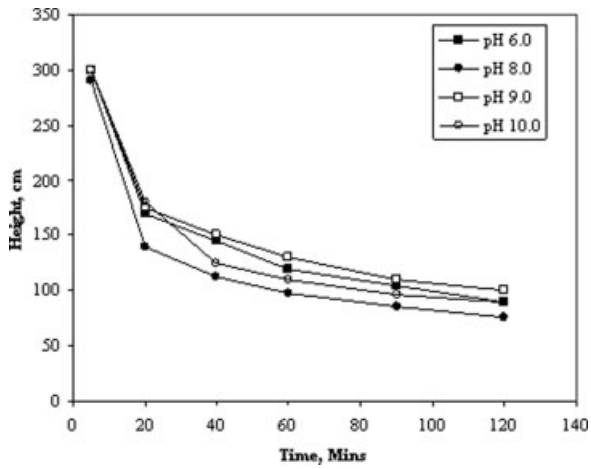

Figure 12. Settling rates of the solids at different pH levels.

Evolution of BET specific surface area

The change in the BET surface area with time is shown in Figure 13. The increase in the surface area from 5 to 40 min for the cases pH 8.0, pH 9.0 and 10.0, and up to 90 min for the pH 6.0 case could have been due to two factors. First, the disappearance of the large particles which produced the second and third peaks in the particle-size distribution could have resulted in an overall increase in the surface area of the particles (see Figures 3 to 6). Second, by considering Figure 2, it can be seen that in the corresponding time intervals for the pH 6.0, pH 8.0 and 9.0 cases, there was a corresponding consumption of supersaturation due to nucleation and a resultant increase in the proportion of smaller particles. This would have the same effect of increasing the BET surface area as in the first instance. The drop in the BET surface area after 40 min and 90 min for the pH 8.0, 9.0, and pH 6.0 cases, respectively, was most likely due to aggregation, resulting in the formation of ferrihydrite flocs. Indeed XRD analyses at these time intervals showed the major component of the precipitates to be ferrihydrite. The traces of green rusts and lepidocrocite, which were detected in the earlier stages could not be detected any more. The decrease in BET surface area at the same point at pH 10.0 could not be explained. The next increase in the BET surface area for all cases could have been due to aging which resulted in the formation of more crystalline phases. Also, sulfate is known to promote the aggregation of ferrihydrite particles and hinder the penetration of nitrogen,[31] a phenomenon that would result in lower BET surface areas. Measurement of the sulfate in solution showed that it was either adsorbed on the precipitate or incorporated in the precipitate, or both, during the early stages of the reaction. As the sulfate was released toward the end of the reaction, the disorder of the particles diminished, resulting in the formation of more crystalline species, and, hence, higher BET specific surface areas. During the earlier stages of the reaction the surface area of the particles formed

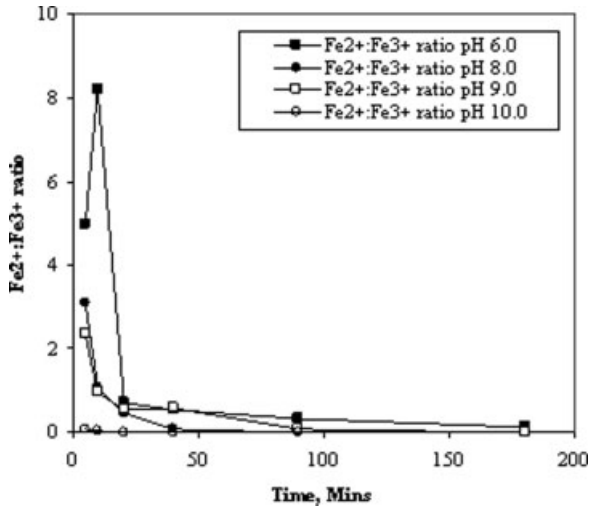

Figure 14. Change in Fe^{2+}:Fe^{3+} ratio with time.

at pH 9.0 was higher than at pH 6.0, in agreement with particle size measurement results. After the aggregation step, the BET surface area of the particles formed at pH 9.0 was lower than for the particles formed at pH 6.0. This could have been due to the presence of Fe^{2+} ions in the precipitate formed at pH 6.0, while the precipitate formed at pH 9.0 was predominantly Fe^{3+} at this stage. The Fe^{2+}/Fe^{3+} composition of the precipitates is shown in Figure 14. Another reason for this trend could be that the extent of aggregation is higher for the pH 9.0 case than for the pH 6.0 case, which resulted in lower BET surface areas. This can also be qualitatively inferred from Figure 9. The fact that there is an initial increase followed by a drop in the BET surface area all cases, and that the drop coincides with the disappearance of the bimodal distribution is very significant. The first significance is that the cycle of reactions that lead to the formation of the final product in the first three cases must be the same; the second is that from a solid-liquid separation point of view it should be technically better to effect solid-liquid separation before the ferrous iron is completely oxidized in the three cases. The final BET specific surface area ($\approx$200 m^2/g) found for the precipitates formed in the pH 6.0, 8.0 and 9.0 cases after 1,440 min is typical of ferrihydrite.[17] The trend in the evolution of the BET specific surface area for both types of solids indicate that regardless of the pH of operation the sequence of reaction steps that lead to the formation of the final product could be the same for these cases, except at pH 10.0. It is also important to mention that the individual specific surface areas have very little meaning since many different ranges have been reported for the same iron phases. For example, Jöhnsson[32] reported surface areas of ferrihydrite of 42.9 m^2/g. More illustrations are found in Cornell and Schwertmann.[11]

Conclusion

The rate of oxidation of Fe^{2+} in ferrous sulfate solutions for the pH 8.0, 9.0 and 10.0 cases is much slower than would be predicted from the rate equation given by Stumm and Lee,[5] Tamura et al.,[24] Deng[33] and Millero et al.[34] The reduction in the rate of oxidation was probably caused by a combination of the formation of solid complexes of Fe^{2+} and ferrihydrite[35] and the high sulfate concentrations.[23,24] At pH 6.0, however, the experimental rate of oxidation was higher than that predicted from literature based calculations (2.1 mg(Fe^{2+})/L/min, and 0.044 mg(Fe^{2+})/L/min, respectively). This increased rate was due to the catalytic effect of the ferrihydrite solids.[23,25] The initial rapid decrease in Fe^{2+} in solution represents direct aqueous oxidation, while the slower one represents the oxidation of complexed Fe^{2+} and Fe^{2+} adsorbed on ferrihydrite solids. This latter stage of the reaction represents the so-called instability of iron hydroxide sludge encountered in the treatment of acid mine drainage. To counter these transformation effects most operations employ a post precipitation stabilization stage before final disposal.[4]

The characteristics of ferric particles formed from homogeneous ferrous sulfate solutions are controlled by the rate of oxidation. High-oxidation rates (achieved by raising the pH) produce high-supersaturation levels, leading to high-primary nucleation rates and the formation of small particles. However, there is competition between deprotonation induced aggregation and nucleation. At pH 6.0, deprotonation dominates and the particles formed are larger in size, whereas at higher pH, although there is more base available for deprotonating the cationic species, the high-oxidation rates dominate, resulting in the formation of smaller particles. However, at pH 8.0, Van der Waals induced aggregation dominates, resulting in the formation of larger particles. At pH 10.0, these stages, which take place during the initial stages of the formation of ferrihydrite, could not be distinguished due to the more rapid kinetics experienced at this pH. The absence of hydroxyl ions necessary for deprotonation explains why Van der Woude and De Bruyn,[12] Pavlides[13] and Dousam and De Bruyn[26] found a limiting size (3–5 nm) for the ferrihydrite particles compared to the several 100 nm obtained in this work. From the evolution of the zeroth moment, it can also be inferred that ferrihydrite size enlargement is aggregation dominated and growth limited. The aggregation is also enhanced around the point of zero charge of the precipitating iron species. Although the final particle sizes obtained in all cases are different, the solids formed have very similar settling characteristics. It seems logical, therefore, to operate acid mine drainage treatment plants employing hydroxide oxidation and precipitation at higher than current pH values as this ensures higher throughput of sludge of the same settling character compared to lower volumes of sludge of the same settling characteristics that would be produced at current (lower) pH values.

Literature Cited

1. Pulles W, Heath R, Howard M.A Manual to Assess and Manage the Impact of Gold Mining Operations on the Surface Water Environment, WRC report No TT79/96. Pretoria, S. Africa, 1996.
2. Kostanbader PD, Haines GF. High density sludge treats acid mine drainage. Coal Age. September 1970;90–97.
3. Bosman DJ. The improved densification of sludge from neutralised acid mine drainage. *J S African Inst Mining Metallurgy*. 1974;340–348.
4. Brown M, Barley B, Wood H. *Minewater Treatment Technology, Application and Policy*. London: IWA Publishing, 2002.

5. Stumm W, Lee GF. Oxygenation of ferrous iron. *Indust Eng Chem*. 1961;53:143–146.
6. Gan WY, Selomulya C, Tapsell G, Amal R. Densification of iron (III) sludge in neutralisation. *Intl J Mineral Processing*. 2005; 76:149–162.
7. Cominco Engineering Services, Ltd.; Water Treatment Technology.- Pilot scale testing of the high density sludge process. Britannia Mine Acid Mine Drainage Treatment. Vancouver, B.C., 1997.
8. Flynn CMJ. Hydrolysis of inorganic iron(III) salts. *Chemical Reviews*. 1984;84:31–41.
9. Jolivet J, Chaneac C, Tronc E. Iron oxide chemistry. From molecular clusters to extended solid networks. *Chem Commun*. 2004;481–487.
10. Blesa MA, Matijevic E. Phase transformations of iron oxides, oxohydroxides, and hydrous oxides in aqueous media. *Adv Colloid Interface Sci*. 1989;29:173–221.
11. Cornell RM, Schwertmann U. *The Iron Oxides; Structure, Properties, Reactions and Uses*. VCH, Weinheim, 1996.
12. Van Der Woude JHA, De Bruyn PL. Formation of colloidal dispersions from supersaturated iron(III) nitrate solutions. II. Kinetics of growth at elevated temperatures. *Colloids Surfaces*. 1983;8:79–92.
13. Pavlides AG. *The Precipitation of Iron Oxy-hydroxides from Ferrous Sulphate Solution*. University of Witswatersrand, Johannesburg, S. Africa, 1995. MSc Thesis.
14. Cornell RM, Giovanoli R, Schneider W. Review of the hydrolysis of iron(III) and the crystallisation of amorphous iron(III) hydroxide hydrate. *J Chem Technol Biotechnol*. 1989;46:115–134.
15. Jambor L, Dutrizac JE. Occurrence and constitution of natural and synthetic ferrihydrite, a widespread iron oxyhydroxide. *Chem Rev*. 1998;98:2549–2585.
16. Van Der Woude JHA, De Bruyn PL. Formation of colloidal dispersions from supersaturated iron(III) nitrate solutions. I. Precipitation of amorphous iron hydroxide. *Colloids Surfaces*. 1983;8:55–78.
17. Schwertmann U, Cornell RM. *Iron Oxides in the Laboratory, Preparation and Characterization*, 2nd ed. Wiley-VCH, Weinheim, 2000.
18. Randolph AD, Larson MA. *Theory of Particulate Processes*, 2nd ed. NewYork: Academic Press, Inc., 1988
19. Bramley AS, Hounslow MJ, Ryall RL. Aggregation during precipitation from solution: A method for extracting rates from experimental data. *J Colloid Interface Sci*. 1996;183:155–165.
20. Ntuli F, Lewis A. The effect of a morphology modifier on the precipitation of nickel powder. *Chem Eng Sci*. 2006;61:5827–5833.
21. Andreassen J, Hounslow MJ. Growth and aggregation of vaterite in seeded-batch experiments. *AIChE J*. 2004;50:2772–2782.
22. APHA, AWWA, WEF. *Standard Methods for the Examination of Water and Wastewater*. Washington, 1998.
23. Sung W, Morgan JJ. Kinetics and product of ferrous iron oxidation in aqueous systems. *Environ Sci Technol*. 1980;14:561–568.
24. Tamura H, Goto K, Nagayama M. Effect of anions on the oxygenation of ferrous ion in neutral solutions. *J Inorg Nuc Chem*. 1976;38:113–117.
25. Tamura H, Goto K, Nagayama M. The effect of ferric hydroxide on the oxygenation of ferrous ions in neutral solutions. *Corrosion Sci*. 1976;16:197–207.
26. Dousma J, de Bruyn P. Hydrolysis-precipitation studies of iron solutions II. Aging studies and the model for precipitation from Fe(III) nitrate solutions. *J Colloid Interface Sci*. 1978;64:154–170.
27. Loan M, Newman OMG, Cooper RMG. Farrow JB, Parkinson, GM. Defining the paragoethite process for iron removal in zinc hydrometallurgy. *Hydrometallurgy*. 2006;81:104–129.
28. Hove M, Van Hille RP, Lewis A. Reaction pathways and mechanisms during the precipitation of iron from acid mine drainage. Manuscript in preparation, 2007.
29. Lewis DG, Schwertmann U. The effect of [OH] on the goethite produced from ferrihydrite under alkaline conditions. *J Colloid Interface Sci*. 1980;78:543–553.
30. Claassen JO, Sanderbergh RF. Particle growth parameters in the precipitation of metastable iron phases from zinc-rich solutions. *Hydrometallurgy*. 2006;84:165–174.
31. Jonsson J, Jonsson J, Lovgren L. Precipitation of secondary Fe(III) minerals from acid mine drainage. *Applied Geochemistry*. 2006; 21:437–445.
32. Jonsson J. *Phase transformations and surface chemistry of secondary iron minerals formed from acid mine drainage*. Umea University, Umea, Sweden, 2003. PhD Thesis.
33. Deng Y. Formation of iron(III) hydroxides from homogeneous solutions. *Water Res*. 1997;31:1347–1354.
34. Millero FJ, Sotolongo S, Izaguire M. The oxidation kinetics of Fe(II) in seawater. *Geochimica et Cosmochimica Acta*. 1987;51:793–801.
35. Jeon BH, Dempsey BA, Burgos WD. Kinetics and mechanisms for reaction of Fe(II) with iron (III) oxides. *Environ Sci Technol*. 2003;37:3309–3315.

Manuscript received Mar. 21, 2007, and revision received June 22, 2007.